Results in Engineering 25 (2025) 103931

Contents lists available at ScienceDirect

Results in Engineering

journal homepage: www.sciencedirect.com/journal/results-in-engineering

Research paper

Design and testing of a test rig for tubular joints hot-spot stress determination

Mohsin Iqbal [a,*], Saravanan Karuppanan [a], Veeradasan Perumal [a], Mark Ovinis [b], Muhammad Iqbal [c]

[a] *Mechanical Engineering Department, Universiti Teknologi PETRONAS, Seri Iskandar, Perak 32610, Malaysia*
[b] *College of Engineering, Birmingham City University, Birmingham B47AP, UK*
[c] *Department of Mechanical Engineering, CECOS University of IT & Emerging Sciences, Peshawar 25000, Pakistan*

ARTICLE INFO

Keywords:
Circular hollow sections (CHS)
Tubular joints
Stress concentration factors (SCFS)
Hot-spot stress (HSS)
Experimental validation
Test rig

ABSTRACT

Circular hollow section (CHS) members are widely used in structural applications due to their high stiffness, low drag, uniform response under various loading directions, and aesthetically pleasing appearance. However, the complex stress and strain behaviour at the intersections of CHS members, known as tubular joints, is challenging to approximate analytically, necessitating numerical methods for analysis. Experimental validation of these models is essential but often requires sophisticated and costly setups that are not readily available. Although extensive research has been conducted on CHS joints, including validation of numerical and empirical models for determining stress concentration factors (SCFs), gaps remain in understanding SCF behaviour under complex loading scenarios. This study introduces a simplified test rig for investigating hot-spot stress and SCF behaviour in CHS joints for mono-, bi-, and tri-planar loading conditions. Loads are applied using dead weights, and responses are measured with strain gauges. The proposed setup has been validated against finite element analysis results. It accommodates joints made of various materials, such as steel, aluminium, or acrylic, and supports the investigation of SCFs under different combinations of axial, in-plane, and out-of-plane bending loads.

1. Introduction

Numerical simulations are increasingly replacing conventional experimental investigations due to their lower cost and ability to rapidly provide detailed insights into complex behaviours. These simulations are widely applied in structural engineering, particularly for complex structures that are difficult to model analytically. However, numerical models, especially of complex structures, must be validated experimentally to ensure the reliability and accuracy of simulation results. Circular hollow section (CHS) members are an example of such structures commonly used in structural applications because of their high strength, stiffness, low drag, and consistent response under multi-directional loading [1–6]. The interfaces of two or more CHS members, commonly referred to as tubular joints, represent the most critical components of such structures. [7,8]. Some studies have focused on reinforced joints [9–13], while others have proposed probability distribution functions for the design of such joints [10,14–16]. Zavaar et al. [17] provided an updated and comprehensive review of research on tubular joints. Typical experimental testing of offshore tubular joints requires a static rig to hold the joint, a loading mechanism, and a data acquisition system to measure the joint's response. Validated finite element (FE) models are then employed for further investigations.

Various studies have utilized sophisticated setups for testing CHS joints, typically involving heavy reaction frames (support structures) and electric hydraulic actuators, which are resource-intensive and expensive. For example, the reaction frames and electric hydraulic actuators used by Pantelides et al. [18], Nadauld et al. [19], Hosseini et al. [20], Lesani et al. [21,22], Deng et al. [23,24], Krishna et al. [25], He et al. [26], Fung et al. [27,28], Tong et al. [29–31], Fu et al. [32], and Rashnooie et al. [33] often include load cells to monitor applied forces, strain gauges to measure stress and strain, and linear variable displacement transducers (LVDTs) to assess deformation. However, equipment such as electric hydraulic jacks, electric actuators, or load cells—may not be readily accessible. Ahmadi et al. [34–36] used a universal testing machine (UTM) to apply axial compressive loads on the central brace of KT-joints, while Xu et al. [37] employed the UTM for

* Corresponding author.
E-mail addresses: mohsin_22005143@utp.edu.my (M. Iqbal), saravanan_karuppanan@utp.edu.my (S. Karuppanan), veeradasan.perumal@utp.edu.my (V. Perumal), mark.ovinis@bcu.ac.uk (M. Ovinis), muhammadiqbal@cecos.edu.pk (M. Iqbal).

https://doi.org/10.1016/j.rineng.2025.103931
Received 4 November 2024; Received in revised form 23 December 2024; Accepted 1 January 2025
Available online 11 January 2025

testing TT-joints. However, the UTM is limited to applying monotonic loads, which were used in the previously mentioned studies, whereas multiplanar loading conditions require the simultaneous application of two or more loads. Several studies have utilized the experimental results from these referenced works to validate their numerical models [38–46].

To address these limitations, a simplified test rig was designed for the static structural testing of CHS joints, focusing on determining hot-spot stress (HSS) and stress concentration factors (SCFs). SCFs are critical parameters for evaluating HSS and the fatigue life of CHS joints using the widely accepted structural hot-spot stress approach. The complex residual stresses due to welding are included in the S-N curves and are not considered in computing SCF [47–49]. A conceptual design of the test rig was developed using computer-aided design (CAD) software Creo Parametric, and structural simulations were performed using ANSYS Workbench. Testing of various tubular joints under uniplanar or multiplanar loading conditions was simulated through finite element analysis (FEA), demonstrating the proof of concept.

2. Methodology

The development of the static test rig for investigating tubular joints involved three key stages: conceptual design, CAD modelling, and static structural simulations. Fabrication of the components was outsourced to a third-party vendor, and the setup was qualified by testing a typical KT-joint. Strain responses were recorded using strain gauges and compared with FEA results. FEA involves discretising a complex object into smaller, manageable elements and solving them to estimate the overall response [50]. Each step is discussed in detail in the following sections.

2.1. Sizing of KT-joint for experimental testing

In practical applications, CHS joints can be substantially large and heavy. For instance, the KT-joint studied by Ahmadi et al. [51] had an estimated weight of 216 kg, based on CAD modelling and assuming a typical steel density of 8000 kg m^{-13}. A sensitivity analysis was performed using FEA to investigate the influence of geometric parameters on SCFs. The analysis revealed that while SCF values change with variations in joint geometry, they remain consistent when using scaled versions of the same joint design. Thus, the SCF of a joint is comparable to that of a scaled model of the joint. Scaling down provides a practical solution, preserving structural behaviour while reducing logistical constraints. Therefore, a scaled-down version of the KT-joint was selected for experimental testing.

The dimensions provided in the literature by Ahmadi et al. [51] were used as a reference for scaling. However, the scaled-down sizes were unavailable locally. Instead of pursuing costly custom machining, readily available off-the-shelf pipe sizes were used. This approach limited direct validation against Ahmadi et al.'s [51] experimental results due to differences in joint size and weight. Nonetheless, the experimental results could still be validated against FEA results from the scaled model, allowing consistent comparisons between simulation and experimental findings and ensuring the robustness of SCF trends within the scaled geometry. The KT-joint used for testing is shown in Fig. 1. Support plates were welded to the ends of the chord and braces, and holes were drilled to allow bolting of the joint to the reaction frame of the test rig. The fabricated joint was subsequently subjected to loads applied to the central brace.

2.2. Design of reaction frame

The conceptual design of the test rig was finalised following detailed numerical simulations to ensure its suitability for the experimental setup. Its design drew inspiration from existing testing rigs, particularly those used in structural assessments of CHS joints, to accurately replicate relevant loading conditions and boundary constraints. However, instead of employing sophisticated infrastructures, a simple reaction frame was designed to securely hold the joint and transfer the applied loads to the ground. The CAD model of the complete test setup is presented in Fig. 2. Slots were incorporated at the interface between the two side assemblies and the lateral beams instead of circular holes to account for manufacturing tolerances. This design choice minimized the risk of introducing residual stresses during the bolting process, which could occur if the bolts were misaligned with the holes or overtightened. These slots ensured a secure fit while minimising stress concentrations at the bolted connections. The reaction frame was further designed to facilitate the simultaneous application of loads in three orthogonal directions, as discussed in the following section.

Detailed drawings (manufacturing data pack) of the test rig were generated from the CAD model. The fabrication of the test rig, along with a typical KT-joint, was completed by Fas Ling Engineering and Trading in Ipoh, Malaysia. After fabrication, the rig was transported and installed at the Centre of Corrosion Research (CCR) at Universiti Teknologi PETRONAS (UTP). The detailed working principle of the rig is

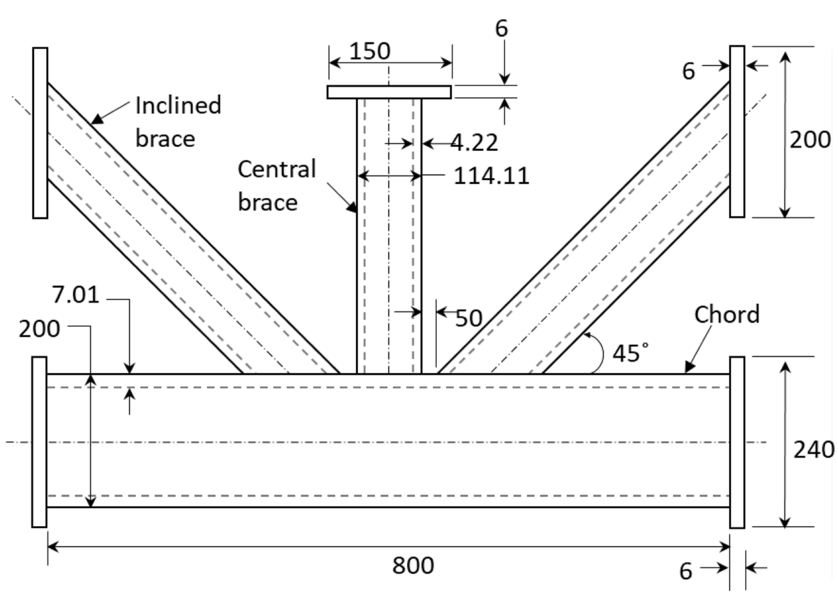

Fig. 1. Dimensions of the KT-joint used for experimentation.

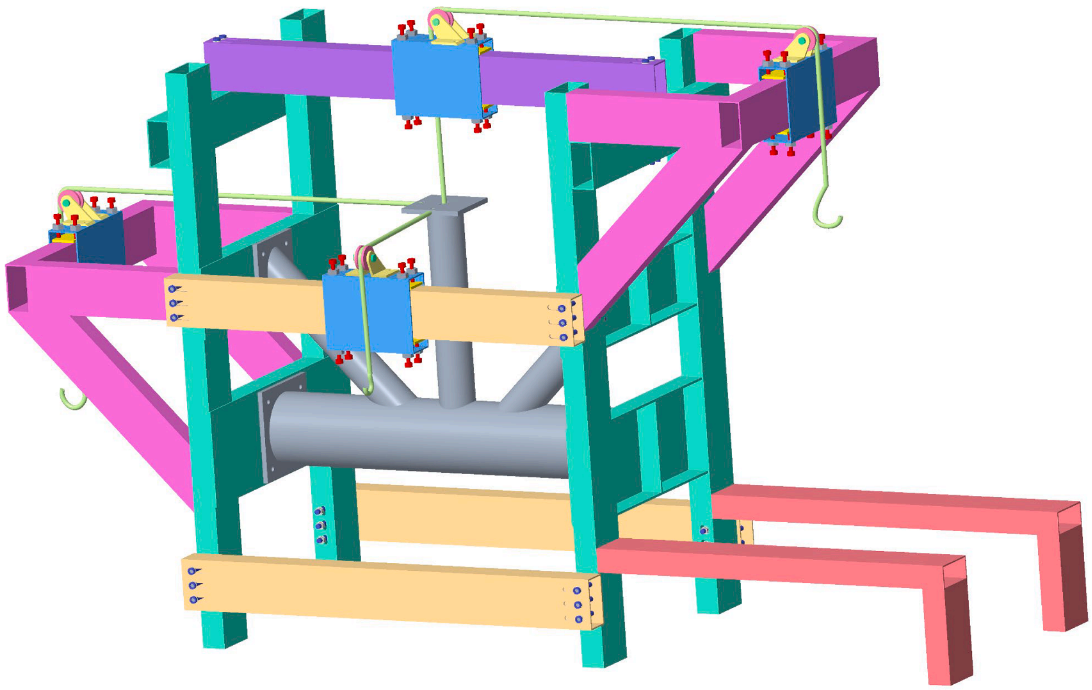

Fig. 2. CAD model of the test rig.

discussed in the following section.

2.3. Finite element analysis

The CAD model of the test rig was simulated in ANSYS Workbench under various combinations of planar loads to ensure its capability to sustain the applied loads. The mesh was generated using nonlinear solid elements, and mesh independence was verified. The final FE model of test rig was consisted of 65,873 elements, as illustrated in Fig. 3. The most severe load configuration occurred when the rig was subjected to simultaneous axial, in-plane bending (IPB), and out-of-plane bending (OPB) loads, as depicted in Fig. 4. Similarly, the KT-joint shown in Fig. 1 was simulated to analyse the stress response of the joint. The model was meshed with high-order solid elements, and mesh independence was ensured through a detailed mesh convergence study. The final FE model including the joint contained 176,138 elements. The joint material was

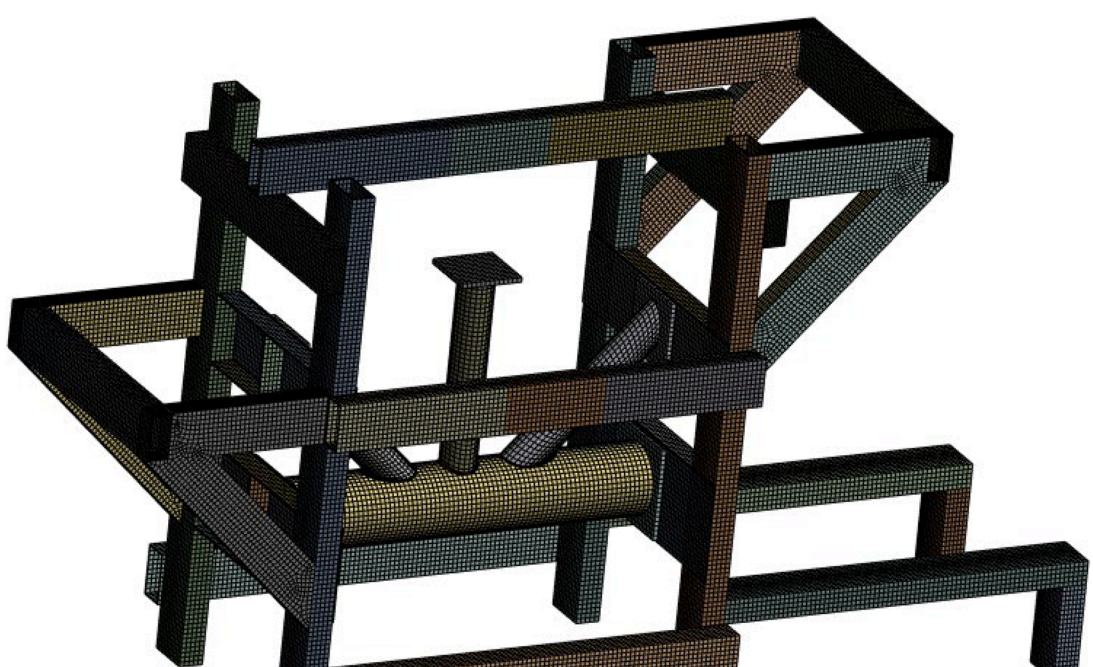

Fig. 3. The finite element model of the test rig and KT-joint.

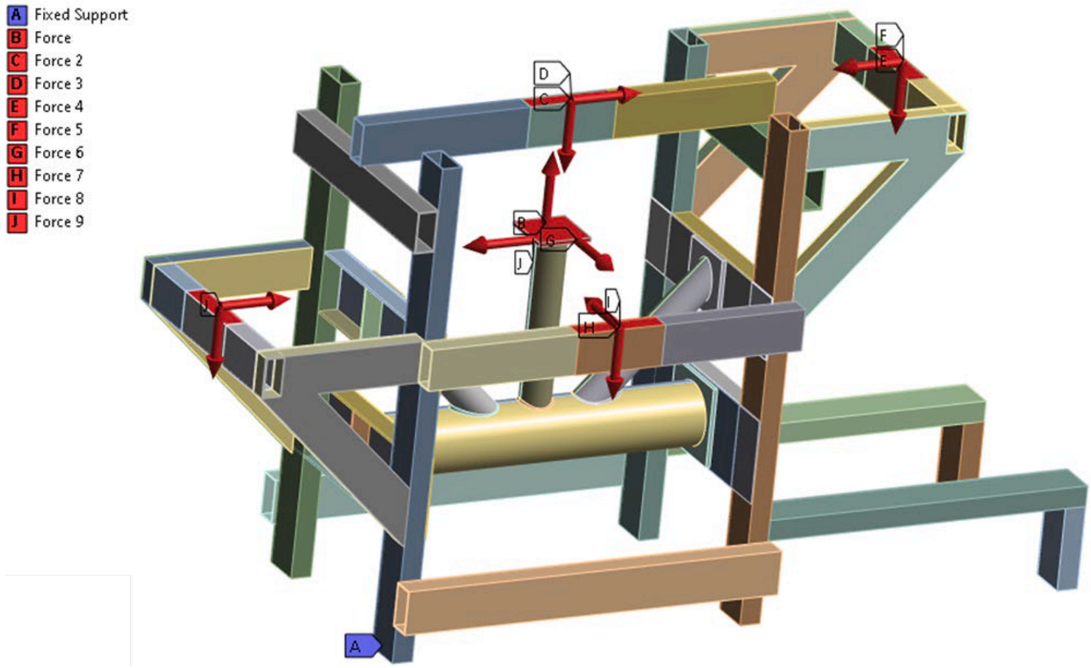

Fig. 4. Boundary conditions used for simulating the test setup.

defined as steel with an elastic modulus of 207 GPa and a Poisson's ratio of 0.3. Boundary conditions included fixed supports at both chord ends and the inclined braces, while the central brace was subjected to a nominal load of 30 MPa. A static structural simulation was performed to determine the stress distribution in the joint. Stresses at 24 circumferential positions around the brace axis were evaluated at two reference points on each position. These stresses were then used to compute HSS at the weld toe through linear extrapolation. The distribution of HSS along the weld toe, measured at intervals of 15°, was used for comparison with the experimentally determined HSS, as detailed in the subsequent section.

Fig. 5. Sand bricks used for the application of load.

2.4. Load application mechanism

The load magnitude was carefully selected to ensure that the deformation of the joint remained within the linear elastic region [37]. A manual lever-operated hydraulic jack equipped with a pressure dial gauge was employed to apply compressive loads. Axial tensile, IPB, and OPB loads were generated using a rope-and-pulley arrangement, adhering to Newton's second law. This mechanism employed 5 mm diameter stainless steel cables and pulleys with negligible rolling friction. Among the various options for dead weights, such as cast iron, stones, sandbags, and bricks, pre-weighted bricks were found to be the most convenient for handling and accessibility during load application. These bricks were wrapped in polyurethane sheets to ensure clean handling and to prevent weight changes caused by erosion of sand or gravel particles. Each brick was weighed using a calibrated scale and appropriately labelled, as shown in Fig. 5 and listed in Table 1. Three steel buckets were suspended from hooks attached to the load cables to accommodate the sand-filled bricks and apply the necessary loads to the joint during testing.

The orientation of the load transfer cable was identified as a critical parameter. Misalignment of the cable can result in unintended multiplanar loads, transferring resultant forces with two or three components instead of a single uniplanar load. Such inaccuracies could significantly impact the recorded stress. Therefore, maintaining accurate cable orientation was crucial to ensuring that the intended loading conditions were applied. To address this issue, a unique pulley adjustment mechanism was implemented to maintain precise orthogonality of the cables during the application of combined (multiplanar) loads, as shown in Fig. 6(a). This mechanism enabled fine-tuning of the pulley angle with millimetre-level precision, ensuring eccentricity control and vertical alignment. Additionally, a laser levelling device with two orthogonal laser beams was employed to further enhance alignment accuracy, as illustrated in Fig. 6(b). This setup ensured precise alignment for accurate load transfer.

2.5. Recording of results

The stress response at extrapolation points was used to determine the hot-spot strain at the interface, which was then converted into the SCF. Two KYOWA linear strain gauges (model # KFGS-2–120-C1–11 L3M2R), featuring a 2 mm gauge length, 119.6 Ω resistance, and 0.9 % thermal sensitivity, were affixed to the joint using KYOWA instantaneous adhesive (model # CC-33A) at 24 positions along the chord around the central brace. Since the maximum principal stress is typically normal to the weld toe [52], linear strain gauges were employed to record the strain response under applied loads. Direct measurement of HSS at the weld toe is challenging due to difficulties in gauge placement and potential weld defects. Therefore, the extrapolation method, as recommended by the CIDECT design guide [53], was employed. While the behaviour of stress could be approximated using linear extrapolation, quadratic extrapolation necessitated an increased number of strain gauges, with even further increases required for higher degrees of extrapolation. Consequently, it is common practice to employ linear extrapolation for determining hot-spot stress in CHS joints, provided that the difference between linear and nonlinear extrapolation is <10 % [54]. Following IIW recommendations [55], strain gauges were installed at distances of 0.4D and 1.4D (D is the chord diameter) from the weld toe linear extrapolation.

Table 1
Weight of sand bricks used for load application.

Block #	Weight (kg)	Block #	Weight (kg)	Block #	Weight (kg)
1	3.000	19	2.980	37	3.015
2	2.995	20	3.000	38	3.080
3	2.940	21	2.775	39	2.890
4	3.000	22	2.870	40	2.715
5	2.960	23	2.780	41	3.000
6	3.025	24	3.090	42	3.960
7	2.970	25	2.755	43	3.140
8	2.880	26	3.000	44	3.000
9	3.000	27	2.970	45	2.965
10	2.830	28	3.000	46	3.000
11	2.775	29	2.955	47	2.980
12	3.025	30	2.790	48	3.000
13	2.950	31	3.000	49	2.950
14	2.960	32	2.970	50	2.920
15	3.000	33	3.020	51	2.810
16	3.040	34	2.845	52	3.050
17	2.975	35	3.005	53	3.000
18	3.000	36	3.000	54	2.980

HSS was recorded at 24 locations along the weld toe of the chord-central brace interface. Before installing the strain gauges, the surface was prepared using sandpaper and cleaned with acetone to ensure that the gauges could bond well. Gauge positions were marked using a CAD-generated template of the developed view in Creo Parametric 9.0, to ensure precise placement, as shown in Fig. 7(a). This drawing was printed at a 1:1 scale, with slits cut at the designated strain gauge positions and pasted onto the chord surface. A narrow-tip brush pen (0.3 mm) was used to mark these positions, as illustrated in Fig. 7(b). These marked lines guided the alignment of strain gauges perpendicular to the weld toe. Strain gauges were oriented perpendicular to the weld toe [37] and affixed at the marked positions following the manufacturer's guidelines. Fig. 8 shows the installed strain gauges, ready for strain measurement.

2.6. Post-processing

In numerical analysis, strains and stresses can be used to calculate strain concentration factors (SNCFs) and SCFs. However, in experimental setups, only strains are measured directly. Nominal strain and hot-spot strain can be converted into stress using Hooke's law, which is valid as long as the material exhibits elastic behaviour [56]. In the experimental setup, strain gauges recorded the strain induced by the applied loads, which was represented in terms of SNCF and converted into SCF using Eq. (1) [57]:

$$SCF = \left(\frac{\varepsilon_{\perp}}{\varepsilon_n}\right) * \left(\frac{1 + \left(\frac{\varepsilon_{\perp}}{\varepsilon_{\parallel}}\right)}{1 - \nu^2}\right) \tag{1}$$

Here, ε_n is the brace nominal strain, $\varepsilon_{\perp}$ is the strain at reference points normal to the weld toe, $\varepsilon_{\parallel}$ is the strain in the direction orthogonal to $\varepsilon_{\perp}$ (tangential to the weld), and ν is Poisson's ratio. The term $(\varepsilon_{\perp}/\varepsilon_n)$ represents the SNCF. Typically, a pair of strain gauges is required at each reference point to measure both normal and tangential strain components for computing SCF. However, due to limitations in the number of strain gauges and the datalogger's recording capacity, only $\varepsilon_{\perp}$ was recorded in this study. To account for the missing tangential strain component, a multiplication factor of 1.15, as recommended by ARSEM design guidelines for offshore structures [58], was applied. The nominal strain on the brace was analytically calculated based on the known applied load, eliminating the need for strain gauges on the brace and avoiding complications associated with nominal bending stress measurement. With this adjustment, Eq. (1) simplifies to Eq. (2):

$$SCF = 1.15 * \left(\frac{\varepsilon_{\perp}}{\varepsilon_n}\right) = 1.15 * \left(\frac{E * \varepsilon_{\perp}}{\sigma_n}\right) \tag{2}$$

Here, E is the Young's modulus of steel, $\varepsilon_{\perp}$ is the hot-spot strain extrapolated from the measured strain at reference points in the direction normal to the weld. The nominal stress σ_n is given by Eq. (3) for axial loading and Eq. (4) for IPB and OPB:

$$\sigma_n = F/A \tag{3}$$

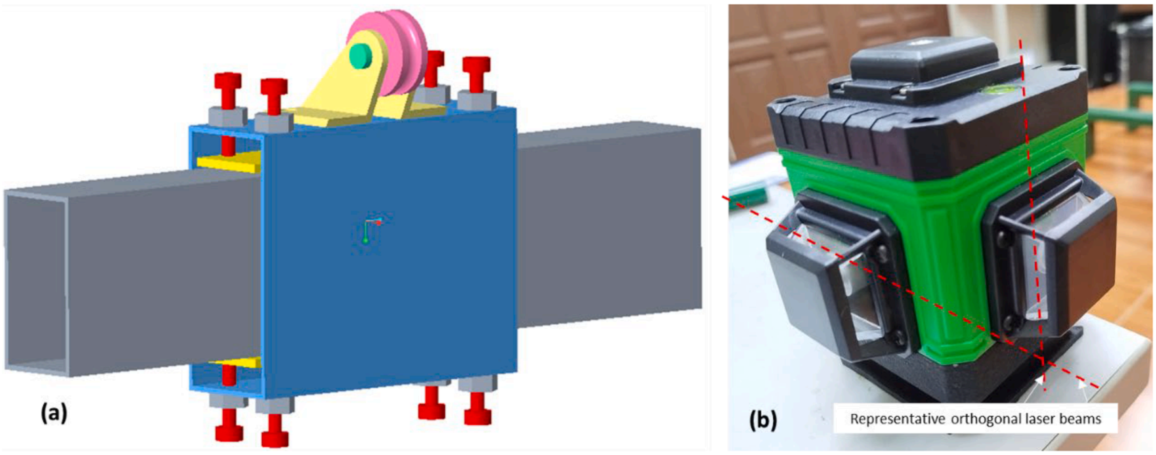

Fig. 6. Mechanism for ensuring load direction (a) adjustment mechanism (b) simulated orthogonal laser beams.

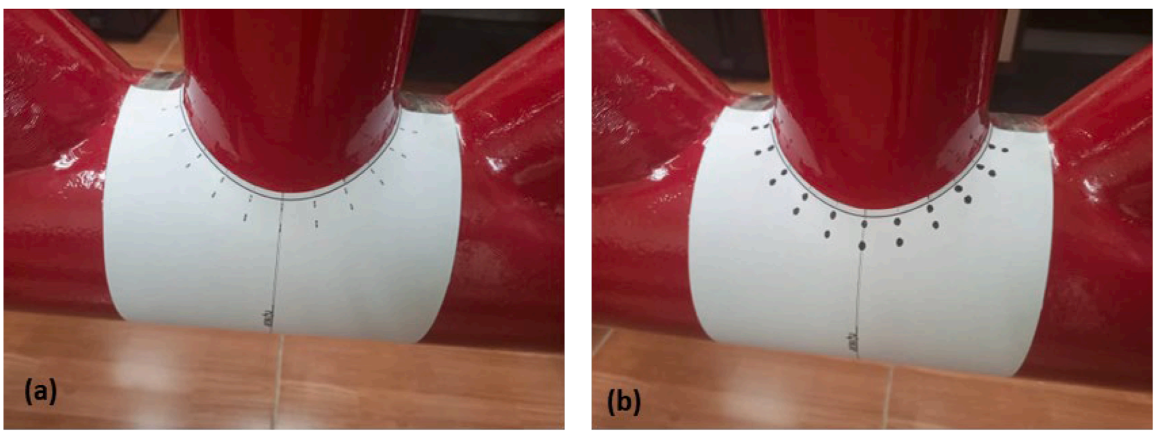

Fig. 7. Installation of strain gauges (a) drawing with slits (b) positions marked.

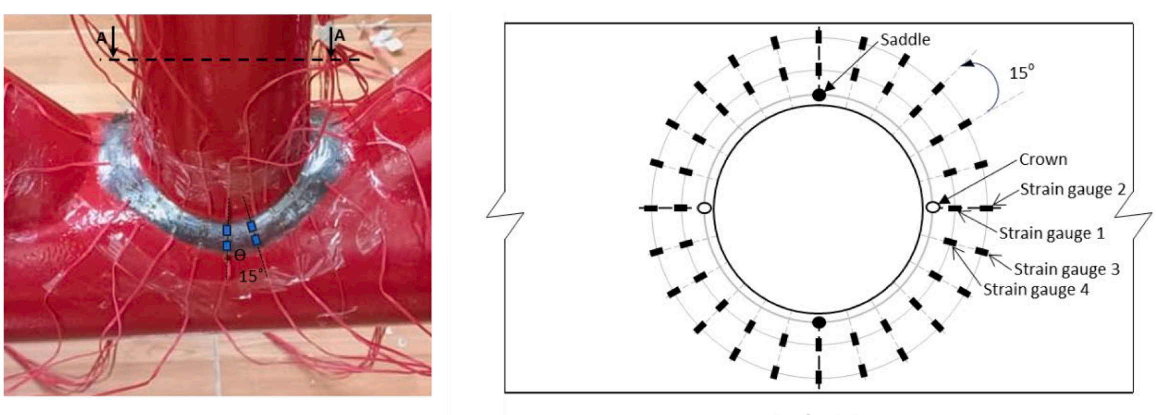

Fig. 8. Strain gauges installed at the interface of the chord and central brace.

$$\sigma_b = 32dM/\left[d^4 - (d-2t)^4\right] \tag{4}$$

Here, F is the applied load, A is the cross-sectional area of the central brace, d is the outer diameter of the central brace, M is the bending moment, and t is the thickness of the central brace. The HSS for combined load cases was computed using the superposition of stresses resulting from individual planar loads, [39].

2.7. Testing of KT-joint

The KT-joint was tested under seven load cases, and SCF values were measured at 24 positions along the weld toe at the chord-central brace interface. The complete test setup is shown in Fig. 9. Data acquisition was performed using a 50-channel datalogger to ensure accurate recording of the strain response. Table 2 presents the load configurations evaluated. The first four tests involved uniplanar loads applied on the central brace, while the last three tests were used to validate the test

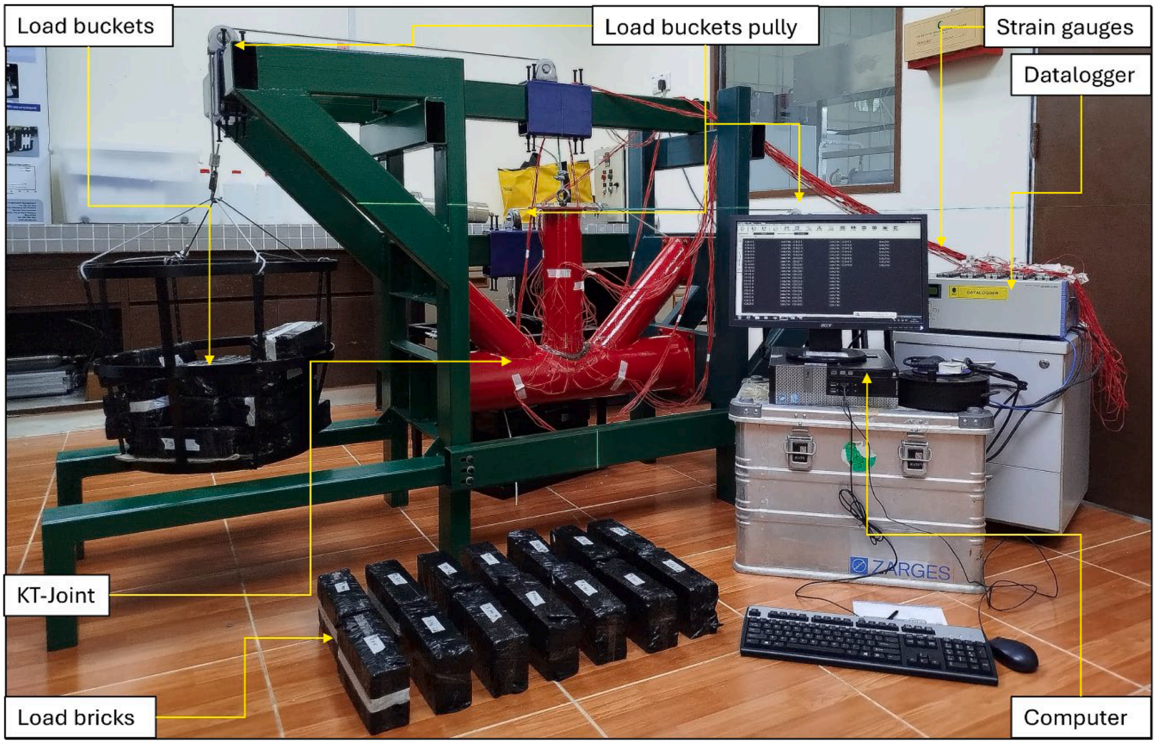

Fig. 9. The static test setup.

Table 2
Details of experimental testing.

S. No.	Description of test/load configuration	Load type
Test 1	Axial compression	Uniplanar
Test 2	Axial tension	
Test 3	In-plane bending (IPB)	
Test 4	Out-of-plane bending (OPB)	
Test 5	Axial tension-IPB	Biplanar
Test 6	Axial tension-OPB	
Test 7	IPB-OPB	
Test 8	Axial tension-IPB-OPB	Tri-planar

rig's multiplanar load capability.

The SCF measurements at the 24 positions along the weld toe of the KT-joint were conducted as follows: Forty-eight channels were activated in the datalogger interface software. The characteristic data of the gauges, provided by the manufacturer were entered into the datalogger interface software, and all connections were verified. The readings were set to zero before applying a preload of 20 %, which was subsequently released to eliminate residual readings. The load was applied incrementally in five steps, with readings recorded at every step to ensure data reliability. In the combined load cases, a constant load of 53.3 kg was applied in one plane, with loads in the second plane at 2:1, 1:1, and 1:2 ratios, using weights of 26.2 kg, 52.8 kg, and 107.3 kg, respectively. A three-minute wait time was observed between load application and data recording to ensure stable readings. The hot-spot strain was determined using stress values at extrapolation points identified through the CAD model in Creo Parametric. Finally, SCF values were calculated via linear extrapolation and plotted against the polar angle about the brace axis, starting from the chord position.

3. Results and discussion

The sizing of the joint was determined based on limits set for deflection and material strength. The maximum von Mises stress recorded in the joint under simultaneous axial tension, IPB, and OPB is shown in Fig. 10. Additionally, it was ensured that the deflection in the test rig remained minimal. The maximum deflection is illustrated in Fig. 11. These results correspond to a dead weight of 1000 kg applied in each direction. Since the SCF is independent of load magnitude, any load lower than this can be safely applied.

While the typical approach in the literature involves validating numerical models with experimental data, this study adopts a reverse methodology: using numerical results to validate the experimental setup. This approach aligns to qualify the test rig design, ensuring it accurately replicates expected stress responses. Validating experimental apparatus using established numerical methods, though less common, is a logical approach when the accuracy of experimental measurements depends on the rig's configuration and boundary conditions.

This reverse validation approach thus provides confidence in the experimental results by aligning them with well-established numerical predictions. The maximum SCF (peak SCF) is used for determining HSS, where difference at this maximum SCF position is critical, while positions with minimal SCF are less consequential. The difference for axial tension and compression was 3.4 % and 3.0 %, respectively, while for IPB and OPB, it was 2.1 % and 3.9 %. These minimal differences confirm the rig's suitability for planar load testing. Fig. 12 presents the experimental and numerical SCF results for various planar axial and bending load configurations.

The rig was used to test the attached KT-joint under multiplanar loads, similar to uniplanar loads. Fig. 13 shows the SCF comparisons for the KT-joint under simultaneous tensile and IPB loads. The magnitudes of these loads were in a 1:2.2 ratio and the peak HSS was observed at 135° and 225°, with a difference of 2.0 %. When the joint was subjected to combined tension and OPB in a 1:2.3 ratio, the peak HSS was noted at 90° with a difference of 2.1 %, as shown in Fig. 14. The KT-joint was also tested for multiplanar bending loads, similar to the combined axial and bending load configurations. Simultaneous IPB and OPB were applied at 1:1, 1:2, and 2:1 ratios, and it was noted that the differences in experimental and numerical results were 7.3 %, 8.5 %, and 4.5 %, respectively. Peak HSS values were observed at 105° for the crown position in the first two load combinations and at 120° for the last load configuration, as

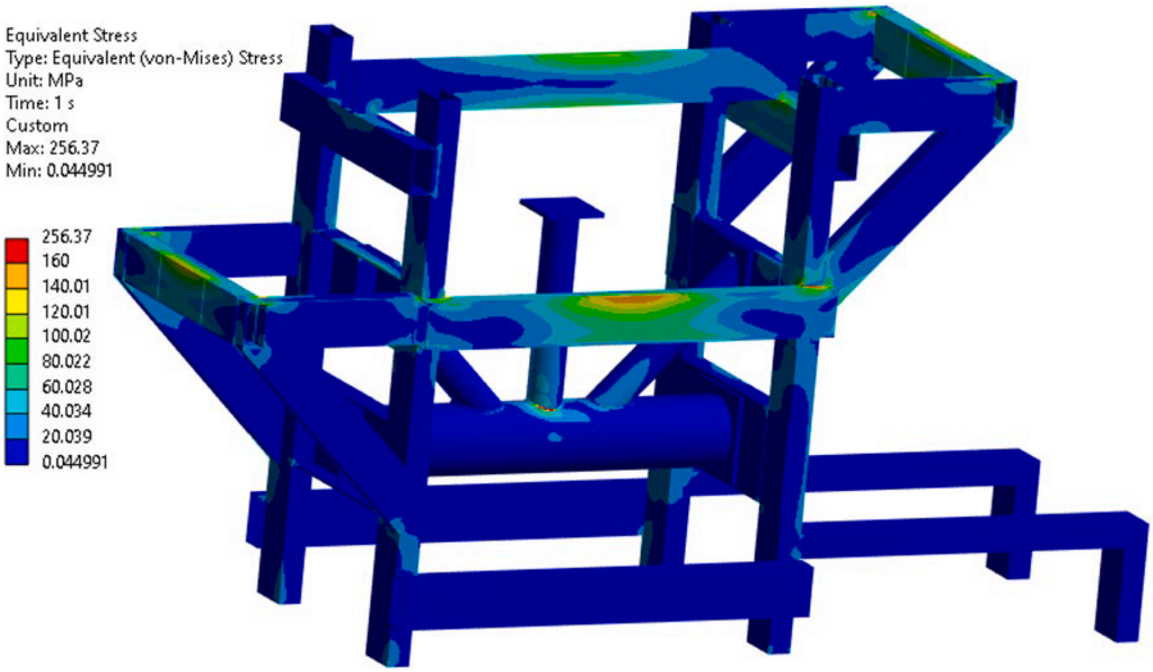

Fig. 10. Maximum Von-Mises stress in the test rig.

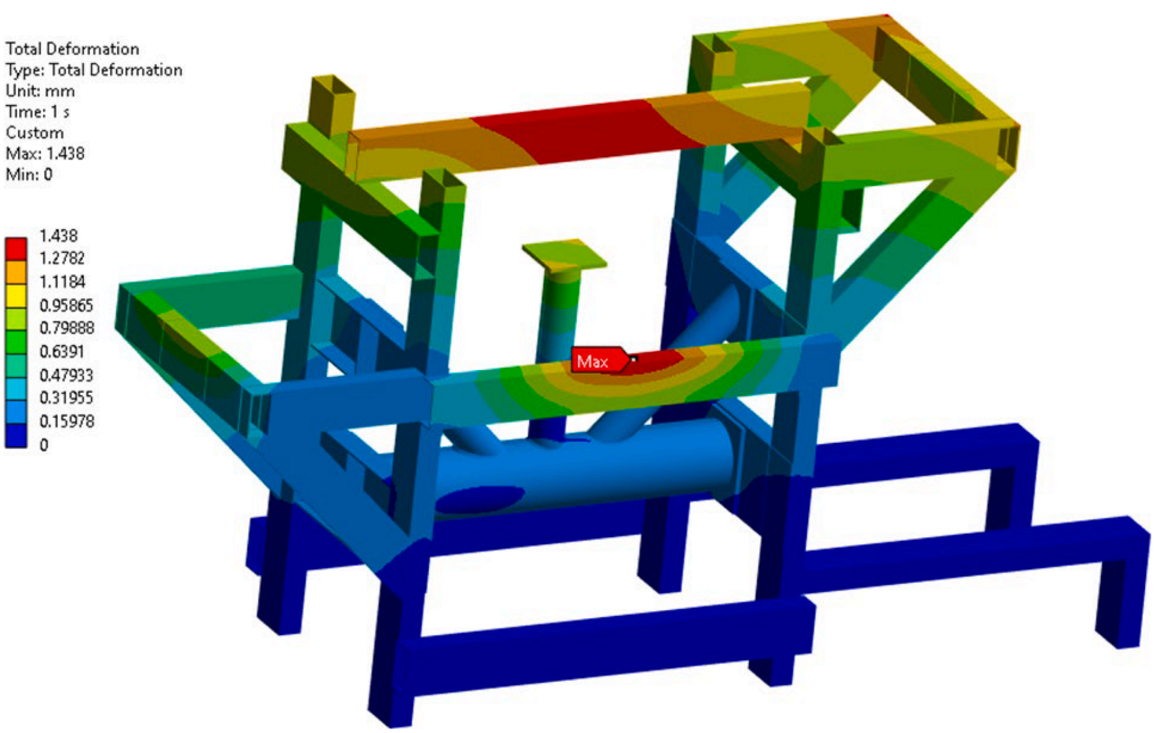

Fig. 11. Maximum deflection in the test rig.

shown in Fig. 15.

This variation in the position of the peak HSS is noteworthy, emphasising the need for an experimental setup and empirical models that have the provision to estimate SCF at various points including the crown and saddle. The developed setup demonstrated the ability to record peak HSS at multiple positions in addition to crown and saddle. This variation in the location of peak HSS highlights the importance of having an experimental setup and empirical models capable of estimating the SCF not only at the crown and saddle points but also at other potential peak locations under multiplanar loading conditions. The developed setup effectively allows for the recording of peak HSS at positions beyond the crown and saddle, ensuring a more comprehensive capture of stress behaviour across the joint.

Finally, the developed setup was used for testing the KT-joint under a tri-planar load configuration comprising axial tension, IPB, and OPB in a 1:6:6 ratio. The peak HSS was observed at 120°, with a difference of 6.9 % between numerical and experimental values, as shown in Fig. 16. Overall, the HSS of typical CHS joints under uniplanar and multiplanar

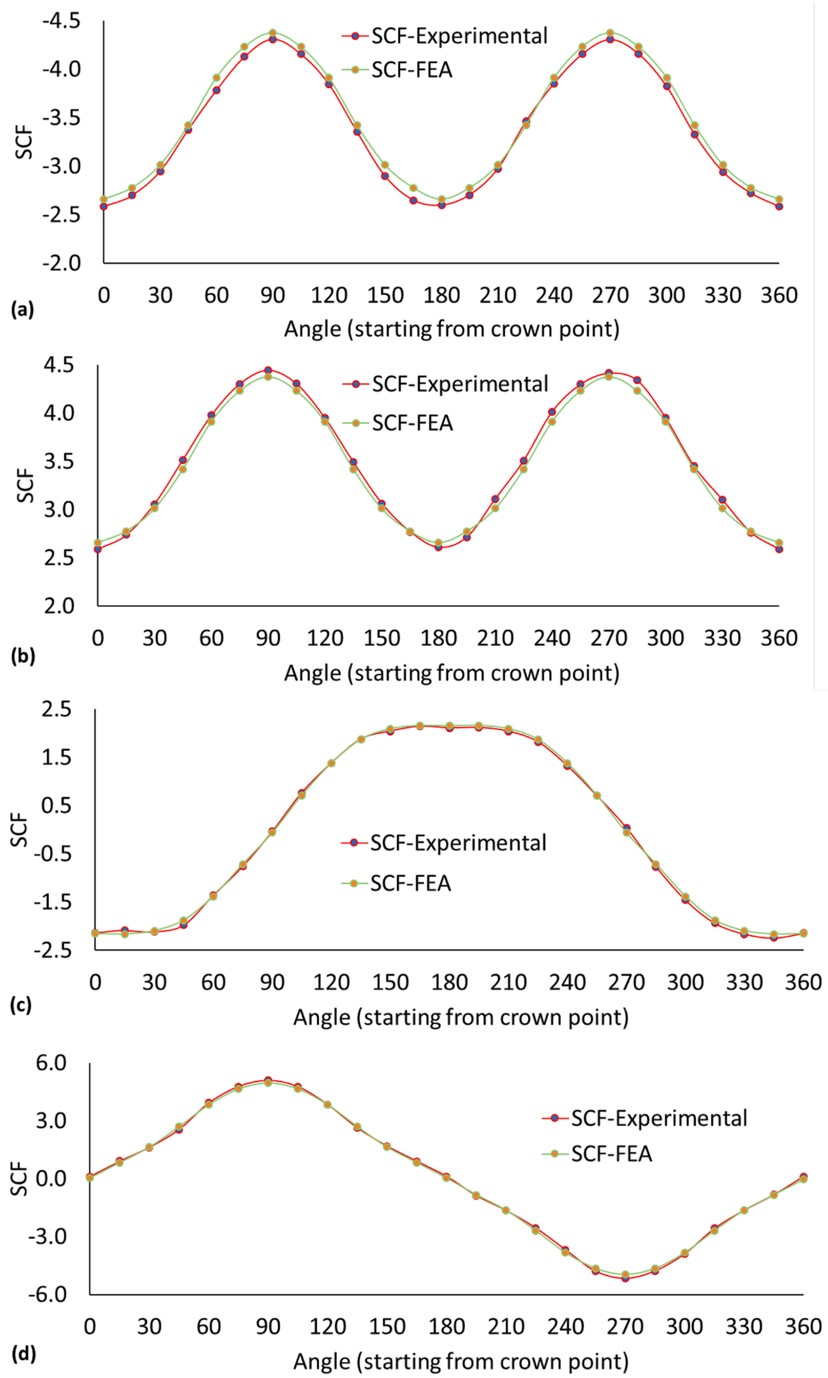

Fig. 12. Experimental and numerical SCF: (a) axial tension (b) axial compression (c) IPB (d) OPB.

load configurations obtained using the test rig were found to closely match numerical predictions.

4. Conclusion

This study presents a simplified experimental setup for investigating hot-spot stress and stress concentration factors in tubular joints under multiplanar loading. Loads were applied using dead weights instead of actuators or universal testing machines. The mechanism for adjusting the load direction was simple and efficient, while load transfer through steel cables proved effective for applying simultaneous planar loads. A typical KT-joint was tested, and the experimental results exhibited less than a 10 % difference compared to numerical predictions, highlighting the reliability of the setup. This versatile configuration is adaptable for testing various tubular joint geometries and load scenarios. Furthermore, it offers the potential for extension to study joints with multiple braces subjected to simultaneous multiplanar loading.

Funding

This research received funding from Yayasan Universiti Teknologi PETRONAS under Grant No 015LC0-443.

CRediT authorship contribution statement

Mohsin Iqbal: Writing – review & editing, Writing – original draft,

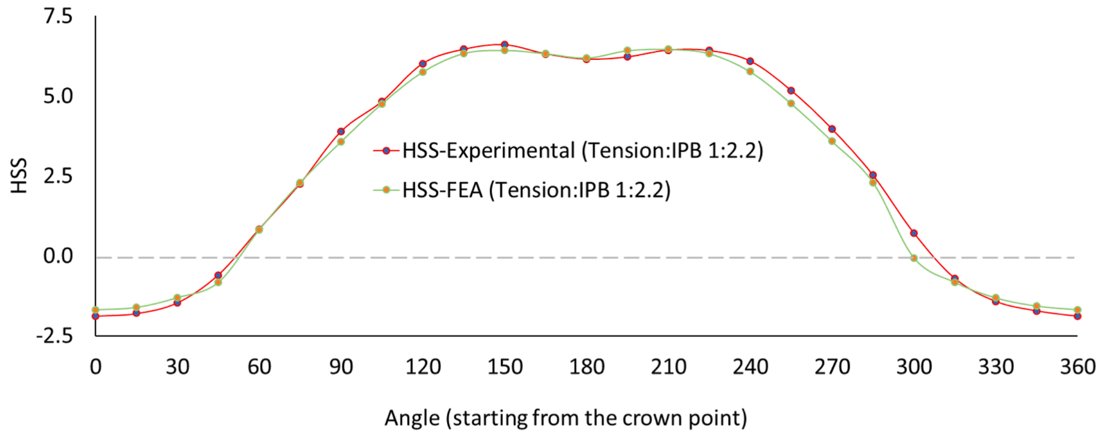

Fig. 13. Experimental and numerical SCFs in KT-joint under Tension-IPB 1:2.2.

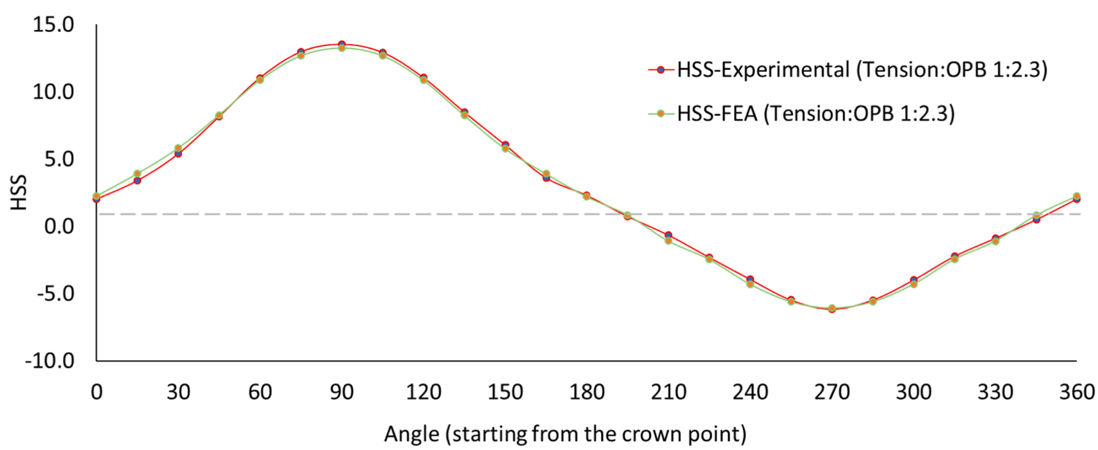

Fig. 14. Experimental and numerical SCFs in KT-joint under Tension-OPB 1:2.3.

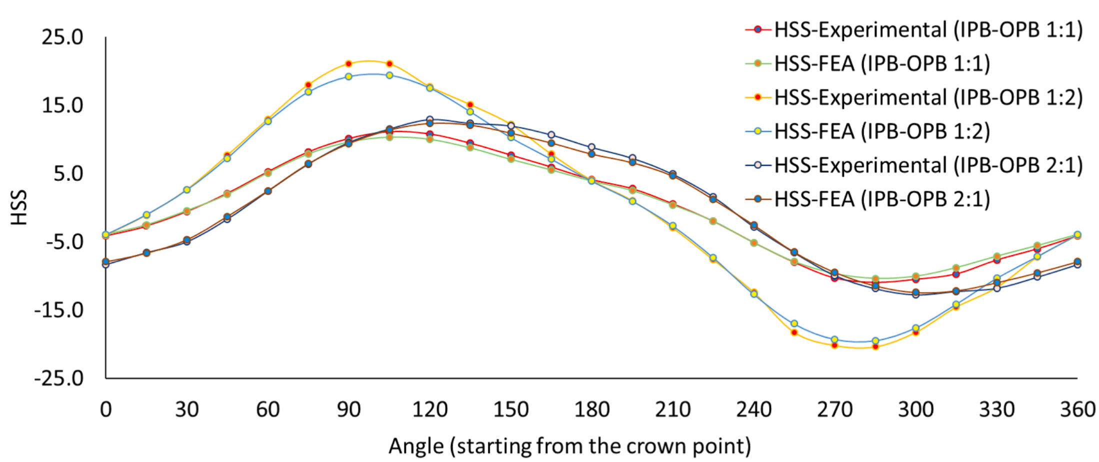

Fig. 15. Experimental and numerical SCFs in KT-joint under IPB-OPB.

Software, Formal analysis. **Saravanan Karuppanan:** Supervision, Project administration, Funding acquisition, Conceptualization. **Veeradasan Perumal:** Supervision, Methodology. **Mark Ovinis:** Writing – review & editing, Supervision, Conceptualization. **Muhammad Iqbal:** Methodology.

Declaration of competing interest

The authors declare that they have no known competing financial interests or personal relationships that could have appeared to influence the work reported in this paper.

Supplementary materials

Supplementary material associated with this article can be found, in the online version, at doi:10.1016/j.rineng.2025.103931.

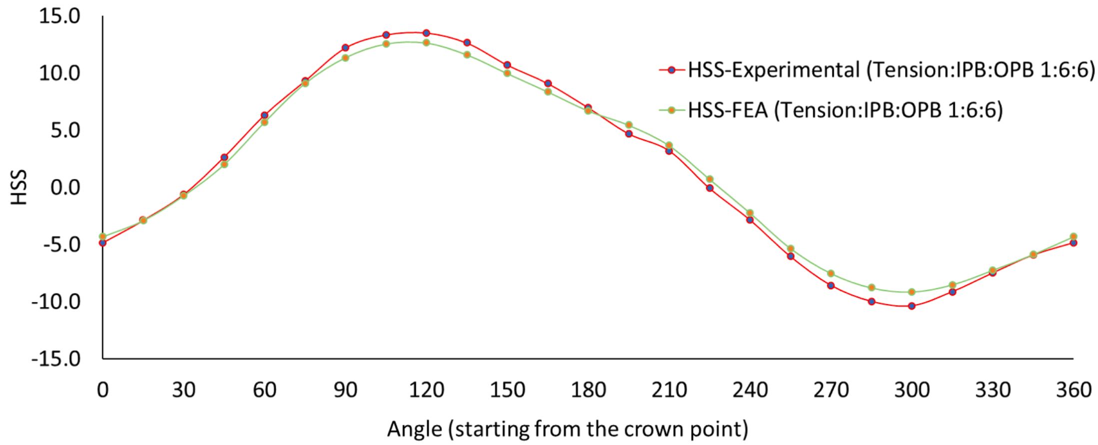

Fig. 16. Experimental and numerical SCFs in KT-joint under axial-IPB-OPB.

Data availability

No data was used for the research described in the article.

References

[1] M. Rabi, F.P.V. Ferreira, I. Abarkan, V. Limbachiya, R. Shamass, Prediction of the cross-sectional capacity of cold-formed CHS using numerical modelling and machine learning, Results Eng. 17 (2023) 100902, https://doi.org/10.1016/j.rineng.2023.100902.

[2] A.A. Kadry, A.M. Ebid, A. Mokhtar A salaam, E.N. El-Ganzoury, S.Y.A. Haggag, Parametric study of Unstiffened multi-planar tubular KK-Joints, Results Eng. 14 (2022) 100400, https://doi.org/10.1016/j.rineng.2022.100400.

[3] A.A. Kadry, A.M. Ebid, E.N. El-Ganzoury, S.Y. Aboul Haggag, A. Mokhtar A salam, Capacity of unstiffened multi-planar tubular KK-gap joints under anti-symmetric loading, Results Eng. 18 (2023) 101092, https://doi.org/10.1016/j.rineng.2023.101092.

[4] E. Zavvar, G. Giannini, F. Taveira-Pinto, P Rosa Santos, Parametric study of stress concentration factors in KT connections reinforced with concrete subjected to axial loads, Ocean Eng. 298 (2024) 117209, https://doi.org/10.1016/j.oceaneng.2024.117209.

[5] T. Wang, L. Tong, F. Gao, X. Xu, W. Shi, M. Pandey, et al., Investigation on load-bearing capacity improvement coefficient of CFRP-reinforced CHS KT-joints, Thin-Walled Struct. 205 (2024) 112455, https://doi.org/10.1016/j.tws.2024.112455.

[6] L. Tong, Y. Wang, L. Gao, W. Shi, F. Gao, Comparative study of different strengthening methods for circular hollow section K-joints, J. Constr. Steel. Res. 217 (2024) 108668, https://doi.org/10.1016/j.jcsr.2024.108668.

[7] M. Iqbal, S. Karuppanan, V. Perumal, M. Ovinis, A. Rasul, Rehabilitation techniques for offshore tubular joints, J. Mar. Sci. Eng. 11 (2023) 461, https://doi.org/10.3390/jmse11020461.

[8] M. Iqbal, S. Karuppanan, V. Perumal, M. Ovinis, A. Rasul, Numerical investigation of crack mitigation in tubular KT-joints using composite reinforcement †, Eng. Proc. 56 (2023) 1–8, https://doi.org/10.3390/ASEC2023-16290.

[9] E. Zavvar, F. Sousa, F. Taveira-Pinto, P Rosa Santos, Multivariate data analysis of maximum stress concentration factors in FRP-retrofitted two-planar KT-joints under axial loads for offshore renewables, J. Mar. Sci. Eng. 12 (2024), https://doi.org/10.3390/jmse12081451.

[10] E. Zavvar, F. Sousa, G. Giannini, F. Taveira-Pinto, P.R. Santos, Probability of maximum values of stress concentration factors in tubular DKT-joints reinforced with FRP under axial loads, Structures 66 (2024) 106809, https://doi.org/10.1016/j.istruc.2024.106809.

[11] E. Zavvar, C.G. Soares, Stress distribution in uniplanar KT joints reinforced with fibre reinforced polymer subjected to the axial loadings, in: Adv. Anal. Des. Mar. Struct. - Proc. 9th Int. Conf. Mar. Struct. MARSTRUCT 2023, Gothenburg, CRC Press, 2023, pp. 565–575, https://doi.org/10.1201/9781003399759-63.

[12] E. Zavvar, J. Henneberg, C Guedes Soares, Stress concentration factors in FRP-reinforced tubular DKT joints under axial loads, Mar. Struct. 90 (2023) 429–452, https://doi.org/10.1016/j.marstruc.2023.103429.

[13] M. Iqbal, S. Karuppanan, V. Perumal, M. Ovinis, A. Khan, Stress concentration factors in CFRP-reinforced KT-joints under multiplanar bending loads: experimental and numerical investigation, Results Eng. 25 (2025) 103745, https://doi.org/10.1016/j.rineng.2024.103745.

[14] E. Zavvar, F. Taveira-Pinto, P Rosa-Santos, Identification of probability distributions of SCFs in three-planar KT-joints, Ocean Eng. 312 (2024) 119222, https://doi.org/10.1016/j.oceaneng.2024.119222.

[15] E. Zavvar, A.G. Majidi, P.R. Santos, F. Taveira-Pinto, Optimal probability distribution for SCFmax in KT-joints strengthened with concrete in wind turbine support structures, J. Constr. Steel. Res. 222 (2024) 108994, https://doi.org/10.1016/j.jcsr.2024.108994.

[16] H. Nassiraei, Probabilistic analysis of strength in retrofitted X-joints under tensile loading and fire conditions, Buildings 14 (2024) 2105, https://doi.org/10.3390/buildings14072105.

[17] E. Zavvar, P. Rosa-Santos, E. Ghafoori, F. Taveira-Pinto, Analysis of tubular joints in marine structures: a comprehensive review, Mar. Struct. 99 (2025) 103702, https://doi.org/10.1016/j.marstruc.2024.103702.

[18] C.P. Pantelides, J. Nadauld, L. Cercone, Repair of cracked aluminum overhead sign structures with glass fiber reinforced polymer composites, J. Compos. Constr. 7 (2003) 118–126, https://doi.org/10.1061/(asce)1090-0268(2003)7:2(118).

[19] J.D. Nadauld, C.P. Pantelides, Rehabilitation of Cracked Aluminum connections with GFRP composites for fatigue stresses, J. Compos. Constr. 11 (2007) 328–335, https://doi.org/10.1061/(asce)1090-0268(2007)11:3(328).

[20] A. Sadat Hosseini, M.R. Bahaari, M Lesani, Experimental and parametric studies of SCFs in FRP strengthened tubular T-joints under axially loaded brace, Eng. Struct. 213 (2020) 110548, https://doi.org/10.1016/j.engstruct.2020.110548.

[21] M. Lesani, M.R. Bahaari, M.M. Shokrieh, Experimental investigation of FRP-strengthened tubular T-joints under axial compressive loads, Constr. Build. Mater. 53 (2014) 243–252, https://doi.org/10.1016/j.conbuildmat.2013.11.097.

[22] M. Lesani, A. Sadat Hosseini, M.R Bahaari, Load bearing capacity of GFRP-strengthened tubular T-joints: experimental and numerical study, Structures 38 (2022) 1151–1164, https://doi.org/10.1016/j.istruc.2022.01.092.

[23] P. Deng, J. Guo, Y. Liu, B. Yang, Damaged tubular T-joints retrofitted with carbon fiber reinforced polymer subjected to monotonic and cyclic loadings, Int. J. Steel Struct. 21 (2021) 299–314, https://doi.org/10.1007/s13296-020-00439-w.

[24] P. Deng, B. Yang, X. Chen, Y. Liu, Experimental and numerical investigations of the compressive behavior of carbon fiber-reinforced polymer-strengthened tubular steel T-joints, Front. Struct. Civ. Eng. 14 (2020) 1215–1231, https://doi.org/10.1007/s11709-020-0663-y.

[25] G.C.S. Krishna, S. Nallayarasu, Experimental and numerical investigation on stress concentration at brace-ring intersection (BRI) of internally ring stiffened tubular T-joints, Appl. Ocean Res. 126 (2022), https://doi.org/10.1016/j.apor.2022.103288.

[26] P. He, M. Pavlovic, Failure modes of bonded wrapped composite joints for steel circular hollow sections in ultimate load experiments, Eng. Struct. 254 (2022) 113799, https://doi.org/10.1016/j.engstruct.2021.113799.

[27] T.C. Fung, T.K. Chan, C.K. Soh, Ultimate capacity of doubler plate-reinforced tubular joints, J. Struct. Eng. 125 (1999) 891–899, https://doi.org/10.1061/(asce)0733-9445(1999)125:8(891).

[28] T.C. Fung, C.K. Soh, T.K. Chan, Erni. stress concentration factors of doubler plate reinforced tubular T joints, J. Struct. Eng. 128 (2002) 1399–1412, https://doi.org/10.1061/(asce)0733-9445(2002)128:11(1399).

[29] L. Tong, G. Xu, X.L. Zhao, H. Zhou, F. Xu, Experimental and theoretical studies on reducing hot spot stress on CHS gap K-joints with CFRP strengthening, Eng. Struct. 201 (2019) 296–313, https://doi.org/10.1016/j.engstruct.2019.109827.

[30] L. Tong, T. Wang, X. Xu, F. Gao, W. Shi, F. Zhou, Experimental study on CFRP reinforcement and static performance of CHS KT-joints, J. Constr. Steel. Res. 216 (2024) 108618, https://doi.org/10.1016/j.jcsr.2024.108618.

[31] L. Tong, G. Xu, X.L. Zhao, Y. Yan, Fatigue tests and design of CFRP-strengthened CHS gap K-joints, Thin-Walled Struct. 163 (2021) 107694, https://doi.org/10.1016/j.tws.2021.107694.

[32] Y. Fu, L. Tong, L. He, X.L. Zhao, Experimental and numerical investigation on behavior of CFRP-strengthened circular hollow section gap K-joints, Thin-Walled Struct. 102 (2016) 80–97, https://doi.org/10.1016/j.tws.2016.01.020.

[33] R. Rashnooie, M. Zeinoddini, E. Ghafoori, M. Sharafi, Experimental and numerical study on the in-plane bending behaviour of FRP-strengthened steel tubular welded T-joints, Thin-Walled Struct. 201 (2024) 112000, https://doi.org/10.1016/j.tws.2024.112000.

[34] H. Ahmadi, E. Zavvar, Degree of bending (DoB) in offshore tubular KT-joints under the axial, in-plane bending (IPB), and out-of-plane bending (OPB) loads, Appl. Ocean Res. 95 (2020) 1187–1206, https://doi.org/10.1016/j.apor.2019.102015.

[35] H. Ahmadi, M.A. Lotfollahi-Yaghin, S Yong-Bo, Chord-side SCF distribution of central brace in internally ring-stiffened tubular KT-joints: a geometrically

parametric study, Thin-Walled Struct. 70 (2013) 93–105, https://doi.org/10.1016/j.tws.2013.04.011.
[36] H. Ahmadi, A. Yeganeh, A.H. Mohammadi, E. Zavvar, Probabilistic analysis of stress concentration factors in tubular KT-joints reinforced with internal ring stiffeners under in-plane bending loads, Thin-Walled Struct. 99 (2016) 58–75, https://doi.org/10.1016/j.tws.2015.11.010.
[37] X. Xu, Y. Shao, X. Gao, H.S Mohamed, Stress concentration factor (SCF) of CHS gap TT-joints reinforced with CFRP, Ocean Eng. 247 (2022) 110722, https://doi.org/10.1016/j.oceaneng.2022.110722.
[38] M. Iqbal, S. Karuppanan, V. Perumal, M. Ovinis, A. Hina, An artificial neural network model for the stress concentration factors in KT-joints subjected to axial compressive load, Mater. Sci. Forum 1103 (2023) 163–175, https://doi.org/10.4028/p-ypo50i.
[39] M. Iqbal, S. Karuppanan, V. Perumal, M. Ovinis, H. Nouman, Empirical modeling of stress concentration factors using finite element analysis and artificial neural networks for the fatigue design of tubular KT-joints under combined loading, Fatigue Fract. Eng. Mater. Struct. 46 (2023) 4333–4349, https://doi.org/10.1111/ffe.14122.
[40] M. Iqbal, S. Karuppanan, V. Perumal, M. Faizan, A. Rasul, M. Iqbal, Modeling stress concentration factors for fatigue design of KT-joints subjected to in-plane bending loads using artificial neural networks, Int. J. Eng. Res. Africa 71 (2024) 79–92, https://doi.org/10.4028/p-zOOom9.
[41] A. Rasul, S. Karuppanan, V. Perumal, M. Ovinis, M. Iqbal, K. Alam, Empirical modeling of stress concentration factors using artificial neural networks for fatigue design of tubular T-joint under in-plane and out-of-Plane bending moments, Int. J. Struct. Integr. 15 (2024) 757–776, https://doi.org/10.1108/IJSI-03-2024-0043.
[42] A. Rasul, S. Karuppanan, V. Perumal, M. Ovinis, M. Iqbal, An artificial neural network model for determining stress concentration factors for fatigue design of tubular T-joint under compressive loads, Int. J. Struct. Integr. 15 (2024) 633–652, https://doi.org/10.1108/IJSI-02-2024-0034.
[43] M. Iqbal, S. Karuppanan, V. Perumal, M. Ovinis, M. Iqbal, A. Rasul, Optimization of fibre orientation for composite reinforcement of circular hollow section KT-joints, Int. J. Struct. Integr. 15 (2024) 717–730, https://doi.org/10.1108/IJSI-04-2024-0054.
[44] M. Iqbal, S. Karuppanan, V. Perumal, M. Ovinis, A. Khan, M. Faizan, Stress Concentration factors in KT-joints subjected to complex bending loads using artificial neural networks, Civ. Eng. J. 10 (2024) 1051–1068, https://doi.org/10.28991/CEJ-2024-010-04-04.
[45] A. Rasul, S. Karuppanan, V. Perumal, M. Ovinis, M. Iqbal, Ultimate strength of internal ring-reinforced KT joints under brace axial compression, Civ. Eng. J. 10 (2024) 1543–1560, https://doi.org/10.28991/CEJ-2024-010-05-012.
[46] A. Rasul, S. Karuppanan, V. Perumal, M. Ovinis, M. Iqbal, Multi-objective optimization of stress concentration factors for fatigue design of internal ring-reinforced KT-joints undergoing brace axial compression, Civ. Eng. J. 10 (2024) 1742–1764, https://doi.org/10.28991/CEJ-2024-010-06-03.
[47] M.A.A. Sikder, Y. Banno, K. Kinoshita, Effect of peening treatment on fatigue strength of welded joints of aged steel, Results Eng. 23 (2024), https://doi.org/10.1016/j.rineng.2024.102781.
[48] B. Laher, C. Buzzi, P. Brunnhofer, M. Leitner, Effect of grinding on the fatigue strength of mild and high strength steel fillet weld joints, Results Eng. 22 (2024) 102135, https://doi.org/10.1016/j.rineng.2024.102135.
[49] D Kollár, Numerical modelling on the influence of repair welding during manufacturing on residual stresses and distortions of T-joints, Results Eng. 20 (2023), https://doi.org/10.1016/j.rineng.2023.101535.
[50] X. Chen, Y. Liu, Finite Element Modeling and Simulation With ANSYS Workbench, CRC Press, Boca Raton, 2015, https://doi.org/10.1201/b17284.
[51] H. Ahmadi, M.A. Lotfollahi-yaghin, S Yong-bo, Experimental and numerical investigation of geometric SCFs in internally ring-stiffened tubular KT-joints of offshore structures, J. Persian Gulf 43 (2013) 7–8.
[52] J. Wardenier, Hollow Sections in Structural Applications, Delft University of TechnologyCIDECT, Netherland, 2001.
[53] X.L. Zhao, S. Herion, J a Packer, R.S. Puthli, G. Sedlacek, J. Wardenier, et al., Design Guide For Circular and Rectangular Hollow Section Welded Joints Under Fatigue Loading, 8, TU Delft, Netherlands, 2001.
[54] Smedley P., Fisher P. Stress concentration factors for simple tubular joints. London: Health and Safety Executive - Offshore Technology Report; 1991.
[55] E. Niemi, W. Fricke, S.J. Maddox, The Structural Hot-Spot Stress Approach to Fatigue Analysis, 2nd Edi, Springer, 2018, https://doi.org/10.1007/978-981-10-5568-3_2.
[56] H. Neuber, Theory of stress concentration for shear-strained prismatical bodies with arbitrary nonlinear stress-strain law, J. Appl. Mech. Trans. ASME 28 (1960) 544–550, https://doi.org/10.1115/1.3641780.
[57] H. Ahmadi, E. Zavvar, Stress concentration factors induced by out-of-plane bending loads in ring-stiffened tubular KT-joints of jacket structures, Thin-Walled Struct. 91 (2015) 82–95, https://doi.org/10.1016/j.tws.2015.02.011.
[58] ARSEM, Design guides for offshore structures - Welded tubular joints, Peris: Technip, Peris France 1 (1987).